EPJ Photovoltaics **4**, 45103 (2013)
www.epj-pv.org
DOI: 10.1051/epjpv/2013014

Feasibility of using thin crystalline silicon films epitaxially grown at 165 °C in solar cells: A computer simulation study

S. Chakraborty[1], R. Cariou[2], M. Labrune[2,3], P. Roca i Cabarrocas[2], and P. Chatterjee[1,2,a]

[1] Indian Association for the Cultivation of Science, 700032 Kolkata, WB, India
[2] Laboratoire de Physique des Interfaces et des Couches Minces, École Polytechnique, 91128 Palaiseau, France
[3] Total S.A., Gas & Power – R&D Division, 92400 Courbevoie, France

Received: 27 July 2012 / Accepted: 15 February 2013
Published online: 9 April 2013

Abstract We have previously reported on the successful deposition of heterojunction solar cells whose thin intrinsic crystalline absorber layer is grown using the standard radio frequency plasma enhanced chemical vapour deposition process at 165 °C on highly doped P-type (100) crystalline silicon substrates. The structure had an N-doped hydrogenated amorphous silicon emitter deposited on top of the intrinsic epitaxial silicon layer. However to form the basis of a solar cell, the epitaxial silicon film must be chiefly responsible for the photo-generated current of the structure and not the underlying crystalline silicon substrate. In this article we use detailed electrical-optical modelling to calculate the minimum thickness of the epitaxial silicon layer for this to happen. We have also investigated by modelling the influence of the a-Si:H/epitaxial-Si and epitaxial-Si/c-Si interface defects, the thickness of the epitaxial silicon layer and its volume defect density on cell performance. Finally by varying the input parameters and considering various light-trapping schemes, we show that it is possible to attain a conversion efficiency in excess of 13% using only a 5 micron thick epitaxial silicon layer.

1 Introduction

The rapid growth of the photovoltaic industry and the resultant shortage of silicon feedstock supply in the last decade, prompted interest in thin crystalline wafers obtained either by thinning down thick ones or by developing epitaxial growth processes. The latter option has gained particular importance [1–3] in view of the fact that the epitaxial silicon film can be "lifted off" from the c-Si substrate (or any other suitable substrate) on which it is grown, and be transferred to a foreign substrate [4], thus allowing for cost-saving via c-Si substrate re-use. In addition, Petermann et al. [4] demonstrated that it is possible to attain ∼19% efficiency in heterojunction solar cells with only a 43 micron thick intrinsic epitaxial silicon layer. However all these approaches involve temperature processes in excess of 600 °C, which limits the range of suitable substrates and often require post-hydrogenation to passivate the defects in the epitaxial silicon layer.

In the wafer equivalent approach used by Cariou et al. [5] the epitaxial silicon (epi-Si) films are deposited in a standard industrial radio frequency plasma enhanced chemical vapour deposition (RF-PECVD) system on highly doped c-Si (100) substrates at 165 °C, allowing for the additional advantage of a low thermal budget with a standard industrial tool. In these epi-Si films high crystalline quality and low stress levels have been confirmed from HRTEM and Raman measurements. At such low growth temperatures it may seem normal for the epitaxial film to have a high density of defects; however a high fill factor of ∼79% has been achieved in ITO/N-a-Si:H/I-epi-Si (1.7 microns)/P^{++}-c-Si/Aluminium type solar cells fabricated from these epi-Si layers, testifying to the excellent quality of the epitaxial films produced. In fact our low temperature material comes with high hydrogen content, which provides de facto good defect passivation. Moreover since for a satisfactory diffusion length, $L_{\mathrm{Eff}} > 3d$, where d is the epitaxial layer thickness, a thinner film demands lower material quality. So far the maximum thickness of the epi-Si layer achieved, retaining good crystalline quality is ∼5 microns.

However to form the basis of a solar cell, the epitaxial silicon (epi-Si) film must be responsible for the photo-generated current of the structure. So far, in this so-called wafer equivalent approach, people made the assumption that the PV response coming from the highly doped wafer is negligible. But, to our knowledge, no quantitative study has been completed to determine whether a part of this

[a] e-mail: parsathi_chatterjee@yahoo.co.in

current is coming from the underlying P^{++}-c-Si substrate, nor has the minimum thickness of the epi-Si layer been determined, so that the major current contribution comes from it. This knowledge is of utmost importance, since our final aim is to achieve a lift-off from the c-Si wafer allowing for the re-use of the latter. As far as the epi-Si film itself is concerned, it has already been demonstrated [6,7] that by using a SiF_4 plasma etching step on the wafer substrate before the deposition of the epi-Si film, it is possible to produce a crystalline silicon layer having a porous interface with the c-Si wafer, which allows the epi-Si film to be easily detached from the substrate. It is naturally desirable that after such detachment, the photo-current of the device remains more or less the same. Also as it is likely that the first few layers of the epi-Si film at its interface with the P^{++}-c-Si may be more disordered, we need to know the minimum thickness of epitaxy required to reduce the defect density at the epi-Si/P^{++}-c-Si interface and thereby to minimise recombination at this interface, as well as to obtain a low defect density inside the epi-Si layer itself. Moreover the maximum open-circuit voltage (V_{oc}) and efficiency achieved so far are 0.55 V and 7% respectively in an actual solar cell having a 2.4 μm thick epi-Si layer and all flat interfaces. Therefore we need to optimise the structure to bring out the potential conversion efficiency achievable in epi-Si solar cells, remembering that it may not be possible (or desirable) to attain a thickness of ~43 μm for the epi-Si films [4] at temperatures below 200 °C, which is the primary advantage of the present method, from the point of view of reduced material cost and low thermal budget.

In order therefore to answer the above questions and in general to study the feasibility of using such thin crystalline silicon films epitaxially grown at 165 °C in solar cells, we have simulated the deposited solar cells using the one dimensional detailed electrical-optical model "amorphous semiconductor device modelling program (ASDMP) [8,9]", to determine the fraction of the total photo-current actually coming from the epi-Si layer. We have also used it to extract the parameters that characterize these devices. Using these parameters to study the sensitivity of the solar cell output to various device and material parameters, we try to pinpoint the parameters to which the solar cell output is most sensitive and whose improvement is essential for the success of epi-Si solar cells. Finally, using the optical model built into ASDMP, we try to predict the maximum efficiency achievable in such structures for a practical thickness of 5 μm for the absorber epi-Si layer.

2 Experimental details

Heavily boron-doped (100)-oriented Si wafers with a resistivity of 0.02−0.05 Ω cm and a thickness of 525 μm were used as substrates for the epitaxial growth, as well as the electrical contact for the solar cell. The native oxide was removed from the surface of the c-Si wafer just before loading it into the multi-plasma monochamber (13.56 MHz) capacitively coupled RF-PECVD reactor [10]. Undoped epitaxial Si layers of various thicknesses (0.9, 1.7 and 2.4 μm) were deposited from the dissociation of 6% silane in a hydrogen gas mixture under a total pressure of 2000 mTorr and a RF power density 60 mW cm^{-2}, resulting in a deposition rate of 1.5 Å s^{-1}. A standard N^+-a-Si:H emitter layer was deposited on top after passivating the epi-Si surface with a thin (~3 nm) intrinsic a-Si:H layer without breaking vacuum and holding the temperature constant at 165 °C throughout the deposition process. The area of the cells (2×2 cm^2 for the largest ones) was defined by sputtering ITO through a shadow mask and evaporating aluminium grid contacts above. More details are given in reference [5]. All interfaces are flat and no light-trapping schemes have been introduced. External quantum efficiency (EQE) and current density-voltage (J-V) measurements under AM1.5 illumination were carried out to determine the solar cell output.

3 Simulation model

The one-dimensional "Amorphous Semiconductor Device Modeling Program (ASDMP) [8]", later extended to also model crystalline silicon and HIT cells [9], solves the Poisson's equation and the two carrier continuity equations under steady state conditions for a given device structure, and yields the dark and illuminated J-V and QE characteristics. The program is ab-initio in its electrical part, which is described in references [11,12]. The expressions for the free and trapped charges, the recombination term, the boundary conditions and the solution technique in this program are similar to the AMPS computer code [13]. The transport over the potential barriers at the contacts if any is by thermionic emission and across the N-a-Si:H/epi-Si heterojunction by both thermionic emission and electron diffusion. This is because in this structure electrons are collected at the N-a-Si:H end and, as will be seen later in Figure 5a, at this hetero-junction the conduction band edge is closer to the Fermi level on the I-epi-Si side than in N-a-Si:H, due to the conduction band discontinuity. This means that the free electron density is in fact higher on the epi-Si side than in N-a-Si:H, resulting also in electron diffusion across this heterojunction. The phenomenon is similar to the "inversion layer" observed at the N-a-Si:H/P-c-Si and P-a-Si:H/N-c-Si heterointerfaces [14]. The gap state model consists of the tail states and two Gaussian distribution functions to simulate the deep dangling bond states in the case of the amorphous layers, while in the epi-Si layer and c-Si substrate the tails are absent. The defect density on the surfaces of the epi-Si film is modelled by a defective layer 5 nm thick. This means that a volume defect density of $\sim 2 \times 10^{17}$ cm^{-3} translates into a surface defect density (N_{ss}) of 10^{11} cm^{-2}.

The generation term has been calculated using a semi-empirical model [15] that has been integrated into ASDMP [8]. Both specular interference effects (for flat surfaces) and diffused reflectance, transmittance and light-trapping effects for structures with textured interfaces, are taken into account. The complex refractive indices of each layer are required as input to the modelling program. Light

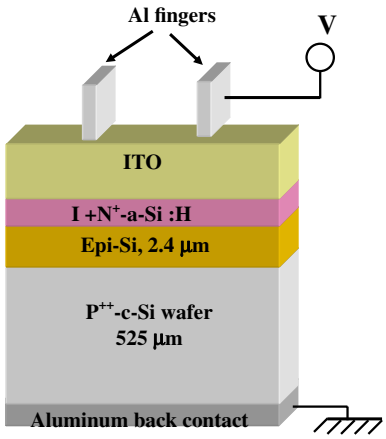

Fig. 1. Schematic diagram of the epitaxial silicon solar cell.

enters through the ITO/emitter "front contact" which is taken at $x = 0$. Voltage is also applied here, while the Al back contact is at earth potential. The P^+-c-Si/Al "rear contact" at the back of the c-Si wafer is taken at $x = L$, where L is the total thickness of the semiconductor layers. The epitaxial c-Si film is assumed to have the same band gap as the c-Si substrate, so that there is only a single hetero-junction (HJ) at the N-a-Si:H/I-epi-Si interface. The top ITO/N-a-Si:H barrier height is assumed to be 0.2 eV, while that of the rear P^+-c-Si/Al is 1.06 eV.

4 Simulation of experiments

The structure modelled is shown in Figure 1. Since the macroscopic structural properties of epi-Si are consistent with c-Si, as deduced from Raman spectroscopy, spectroscopic ellipsometry and transmission electron microscopy measurements [5], the band gap and the complex refractive indices of the epi-Si layer are assumed to be the same as that for c-Si. Therefore this cell has only a single band discontinuity at the N-a-Si:H/I-epi-Si junction. Since it has been shown [16–18] that for an a-Si:H layer deposited via PECVD on c-Si (or, in this case on the epi-Si layer), the major part of the band offset is on the valence band side, we have apportioned two-thirds of the band discontinuity onto the valence band, and the rest onto the conduction band. This large valence band discontinuity (ΔE_v) at the N-a-Si:H/epi-Si junction has a beneficial influence on carrier collection, as it produces a strong field on the photo-generated holes at this junction in the right direction, viz., towards the back of the device, where holes are collected in this structure. Figure 2 compares the experimental illuminated J-V characteristics of epi-Si solar cells of three different thicknesses: 2.4 μm, 1.7 μm and 0.9 μm to model results, while Figure 3 compares the external quantum efficiency (EQE) of the two thicker cells and the reflection from the 2.4 μm cell to our simulations. In Table 1 we compare the measured and calculated solar cell output parameters.

In order to base our model predictions and sensitivity calculations on realistic device parameters, we have modelled the light J-V and EQE characteristics mentioned above. Table 2 and its caption present the input parameters extracted from the above modelling. Of course the parameters marked by superscript "a" in Table 2, such as the thickness of the individual layers, the band gap, the doping and defect densities inside the emitter (deduced from measured activation energies), and the carrier mobilities in the epi-Si layer and the highly doped defective P^+-c-Si wafer have been measured. The doping density in the P^+-c-Si wafer (marked by superscript "c") has been supplied by the manufacturer, while yet other parameters, marked by superscript "b" in Table 2, have been taken from the literature. The main parameters obtained by fitting the measured illuminated J-V and EQE curves

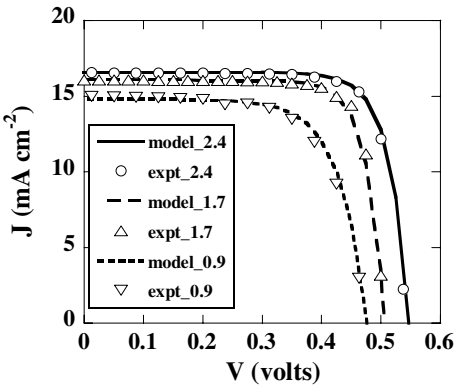

Fig. 2. The experimental (expt) and simulated (model) illuminated J-V characteristics of the epi-Si NIP cells, where the thickness of the epi-Si layer is 2.4 μm, 1.7 μm and 0.9 μm.

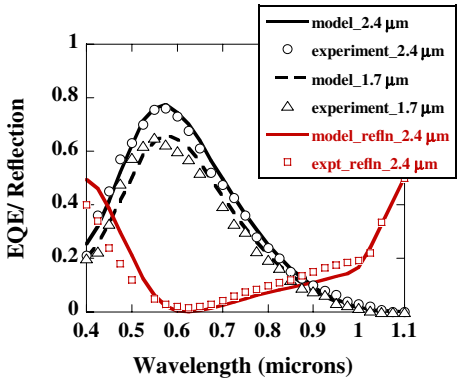

Fig. 3. The experimental (expt) external quantum efficiency (EQE) curves of the 2.4 μm and 1.7 μm epi-Si NIP cells and the reflection from the 2.4 μm device (symbols) under AM1.5 light, 0 V, compared to model results (lines).

Table 1. Comparison of the measured and simulated solar cell output parameters for the deposited epi-Si solar cells.

Case		J_{sc} (mA cm^{-2})	V_{oc} (V)	FF	Efficiency (%)
2.4 μm cell	experiment	16.6	0.546	0.77	7.0
	model	16.6	0.547	0.778	7.07
1.7 μm cell	experiment	16.1	0.510	0.786	6.4
	model	16.1	0.507	0.786	6.4
0.9 μm cell	experiment	15.0	0.478	0.66	4.7
	model	14.8	0.476	0.70	4.95

Table 2. The input parameters used to model the 2.4 μm epi-Si layer cell. Note that the quantities marked with superscript "a" have been measured, those marked with superscript "b" have been taken from the literature, and that marked with superscript "c", supplied by the manufacturer. The other parameters and the interface defect densities have been extracted by simulation. In this case (2.4 μm cell), the defect density at the top N-a-Si:H/I-epi-Si interface is 10^{11} cm^{-2}, while that at the rear I-epi-Si/P$^+$-c-Si interface is 10^{12} cm^{-2}. For the case of the 1.7 μm cell all parameters are the same as for the 2.4 μm cell, only the N-a-Si:H layer appears to be ∼16 nm from modelling (as explained in the text) and the rear interface defect density is higher: 1.35×10^{12} cm^{-2}. However, for the 0.9 μm cell the defect density at both interfaces of the epi-Si layer had to be equal to 10^{12} cm^{-2} and the volume defect density 1.2×10^{16} cm^{-3}. The charged and neutral capture cross-sections (σ) of these defect states, have been assumed to be one order of magnitude higher than the corresponding σ's inside the volume of epi-Si for all cases, while a 0.5 μm region adjacent to the top DL is assumed to have σ's intermediate between the two and a defect density twice that in the rest of the volume.

Parameters	N-a-Si:H	I-epitaxial Si	P-c-Si
Thickness (μm)[a]	0.012	2.4	525
Mobility gap (E_μ) (eV)	1.8[a]	1.12[a,b]	1.12[b]
Doping density (cm^{-3})	1.1×10^{19}[a]	0	3.0×10^{18}[c]
Electron affinity (eV)[b]	4.0	4.22	4.22
Eff. DOS in bands N_c[b]	2×10^{20}	2.8×10^{19}	2.8×10^{19}
(cm^{-3}) N_v[b]	2×10^{20}	1.04×10^{19}	1.04×10^{19}
Charac. En. E_D (E_A) (eV)[b]	0.05 (0.03)	–	–
G_{D0}, G_{A0} (cm^{-3} eV^{-1})[b]	4.0×10^{21}	–	–
Elec. (hole) mobility	20 (4)	400 (125)[a]	300(100)[a]
(cm^2/V S)			
Gaussian defect den. (cm^{-3})	6.0×10^{18}[a]	10^{15}	6.0×10^{17}
Donor Gaussian peak pos	0.7	0.4	0.4
w.r.to VB (eV)			
Acceptor Gaussian peak pos	0.6	0.4	0.4
w.r.to CB (eV)			
Capture cross-sections (cm^2)			
mid-gap: charged (neutral)	10^{-14} (10^{-15})	10^{-16} (10^{-17})	4×10^{-17} (4×10^{-18})
tails: charged (neutral)	10^{-14} (10^{-15})	–	–

therefore are the defect densities at the front and back of the epi-Si layer and the defect density in the volume of this layer. The charged and neutral capture cross-sections (σ) of these defect states, have been assumed to be one order of magnitude higher than the corresponding σ's inside the volume of epi-Si for all cases; while a 0.5 μm region adjacent to the top DL is assumed to have σ's intermediate between the two and a defect density twice that in the remainder of the epi-Si film. Without this latter assumption, we find that the V_{oc} and FF of the cells are overestimated. The defect densities at different points of the structure were extracted in the following way:

In order to fix the defect density at the I-epi-Si/P$^+$-c-Si interface in the 2.4 μm epi-Si layer cell, it was noted that a value of $N_{ss,\,back} \leqslant 7\times10^{11}$ cm^{-2}, leads to a higher V_{oc} but a *lower* FF than the experimental case. A higher V_{oc} for lower $N_{ss,\,back}$ is to be expected, but the lower FF is not. This fact will be explained in detail in Section 5.3.1. Moreover all aspects of solar cell performance deteriorate for $N_{ss,\,back}$ higher than 10^{12} cm^{-2} (Tab. 3). This prompted us to fix $N_{ss,\,back}$ for the 2.4 μm device at 10^{12} cm^{-2}, while the lower V_{oc} of the 1.7 μm device could be matched by assuming a higher $N_{ss,\,back}$ of 1.35×10^{12} cm^{-2} for this case. On the other hand, there is practically no sensitivity of the solar cell output to $N_{ss,\,front}$ (Tab. 3) upto $N_{ss,\,front} = 10^{12}$ cm^{-2}; V_{oc} and FF begins to deteriorate rapidly for higher values of $N_{ss,\,front}$. Therefore our choice of $N_{ss,\,front} = 10^{11}$ cm^{-2} at the top N-a-Si:H/I-epi-Si interface for the solar cells with 2.4 μm and 1.7 μm I-epi-Si layers has been dictated by the fact that for these cases the defects at this hetero-interface have been carefully passivated by depositing a 3 nm thick intrinsic a-Si:H layer on epi-Si before the deposition of the emitter N-a-Si:H. However for the 0.9 μm device, it was found that a front interface defect density less than 10^{12} cm^{-2} leads to a slight over-estimation of V_{oc} and FF and so this latter value was taken as $N_{ss,\,front}$ for the 0.9 μm epi-Si case. On the other hand there is considerable sensitivity of V_{oc} and FF to the Gaussian defect density inside the epi-Si layer beginning from a low value of 10^{14} cm^{-3} for this parameter. Therefore this parameter could be fixed more uniquely and we extracted values of 10^{15} cm^{-3}, 10^{15} cm^{-3} and 1.2×10^{16} cm^{-3} for the 2.4 μm , 1.7 μm and 0.9 μm devices respectively. However as already stated in all cases, a 0.5 μm region next to the top DL had to be assumed more defective with higher σ's (Tab. 2 caption) than in the rest of the epi-Si film to ensure that the model calculations do not overestimate the V_{oc} and FF. It maybe relevant here to point out that the EQE curves in Figure 2 did not help us much in determining the defect densities at different points of the device. It was in fact found that the short wavelength QE (SWQE) right up to the peak EQE were determined, for a given thickness of the flat ITO window layer, by the thickness of the N-a-Si:H emitter and the capture cross-sections of its defect states. The EQE beyond the peak was determined by the thickness of the epi-Si layer. From these arguments one would expect the same SWQE for both the 2.4 μm and the 1.7 μm cells.

Table 3. Sensitivity to the defect density at the rear epi-Si/P-c-Si interface ($N_{ss,\,back}$) and to that at the front N-a-Si:H/epi-Si interface ($N_{ss,\,front}$).

$N_{ss,\,front}$ (cm^{-2})	$N_{ss,\,back}$ (cm^{-2})	2.4 μm cell			
		J_{sc} (mA cm^{-2})	V_{oc} (V)	FF	Efficiency (%)
10^{11}	10^{10}	16.63	0.592	0.748	7.37
	10^{11}	16.63	0.591	0.749	7.36
	5×10^{11}	16.63	0.582	0.758	7.34
	10^{12}	16.63	0.547	0.778	7.07
	5×10^{12}	16.61	0.394	0.663	4.35
	10^{13}	16.60	0.360	0.629	3.76
10^{10}	10^{12}	16.63	0.547	0.778	7.07
10^{11}		16.63	0.547	0.778	7.07
5×10^{11}		16.68	0.546	0.778	7.09
10^{12}		16.75	0.542	0.780	7.09
5×10^{12}		16.77	0.404	0.648	4.39
10^{13}		16.41	0.369	0.596	3.61

As this is not the case (Fig. 2), we had to assume that the N-a-Si:H emitter is thicker – 16 nm instead of 12 nm for the 1.7 μm cell. A 12 nm N-a-Si:H layer with higher capture cross-sections for the 1.7 μm cell was found to yield the same solar cell output, but the EQE is over-estimated.

In summary it has been shown that the defect density at the top N-a-Si:H/I-epi-Si interface is 10^{11} cm^{-2}, while at the rear I-epi-Si/P-c-Si interface it is 10^{12} cm^{-2} for the 2.4 μm cell, as inferred from modelling. In the case of the 1.7 μm cell all parameters, including the defect density inside the epi-Si layer are the same as for the 2.4 μm cell; only the N-a-Si:H layer appears to be ∼16 nm and the rear interface defect density is higher: 1.35×10^{12} cm^{-2}. However for the 0.9 μm cell, the interface defect density at both interfaces had to be taken as equal to 10^{12} cm^{-2}; as well the volume defect density inside the epi-Si layer was found from modelling to be more than 1 order of magnitude higher: $\sim 1.2 \times 10^{16}$ cm^{-3}. Clearly the epi-Si layer has to be at least 1.7 μm thick and preferably more than ∼2 μm thick for good photovoltaic (PV) performance. This point will be discussed further in Section 5.2.

5 Results and discussion

In this section we will first try to understand the origin of the photo-generated current – whether mainly from the epi-Si layer or from the c-Si wafer. We will also try to understand at what thickness of the epi-Si layer does the main contribution to the photo-current come from it. We will also try to determine the optimum thickness of the epi-Si layer for the highest cell efficiency. Thereafter, the sensitivity of the solar cell output to the defect states on the top surface of the epi-Si film (facing the emitter layer), the rear surface (contacting with the doped P^+-c-Si wafer), and the volume defect density inside the epi-Si film, will be investigated.

It may be noted from Table 1 that the epitaxial solar cells have J_{sc} and V_{oc} lower than those of the standard diffused P/N junction mono-c-Si solar cell, while the fill factor (FF) is comparable. One obvious reason for the rather low J_{sc} is that in the present calculations all interfaces are assumed to be flat, resulting in current losses in the poor quality P^+-c-Si wafer. In other words, no light-trapping schemes are included. We will therefore study by modelling the influence of texturing the top and bottom faces of the epi-Si film on J_{sc}. Regarding the low V_{oc}, one reason is surely the rather high defect density at the epi-Si/P-c-Si interface in our solar cells. Here there is no band discontinuity, and holes photo-generated inside the c-Si substrate can easily back diffuse to give a high recombination at this interface when the defect density here is high as is the case for all the deposited cells ($N_{ss} \geqslant 10^{12}$ cm^{-2}). Other factors like the volume defect density in the epi-Si layer itself may also play a role. Finally we need to investigate whether an inversion of the structure by growing the epi-Si layer on an N-type instead of on a P-type c-Si substrate can lead to the possibility of a higher V_{oc}. We will investigate or comment on these factors in the following sections.

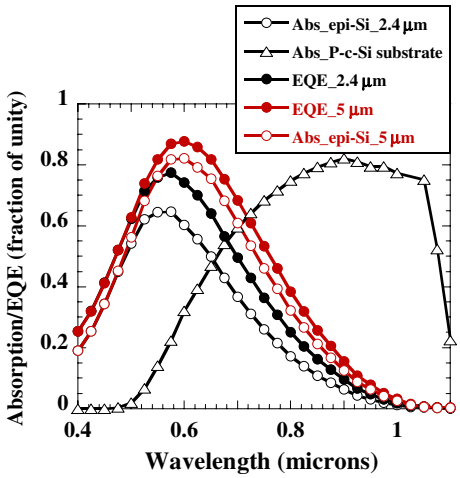

Fig. 4. Model calculations of the absorption (Abs) in the 2.4 μm epitaxial silicon (epi-Si) layer and the P-type c-Si substrate (black lines with open circles and open triangles respectively) and the external quantum efficiency (EQE – black line with closed circles) of the 2.4 μm cell. Also shown are the calculated values of the absorption in the epi-Si layer (red line with open circles) and the EQE (red line with closed circles) if the epi-Si layer were to be 5 μm thick.

5.1 Origin of photo-generated current in these structures

In order to understand the origin of the photo-generated current in this structure – whether mainly from the epi-Si layer or from the c-Si wafer – we plot in Figure 4 the absorption profile in the epi-Si and c-Si layers as well as the external quantum efficiency of the 2.4 μm cell. We note that a significant contribution to the peak EQE comes from the heavily doped P^+-c-Si wafer, which has however been assumed defective. This latter fact is

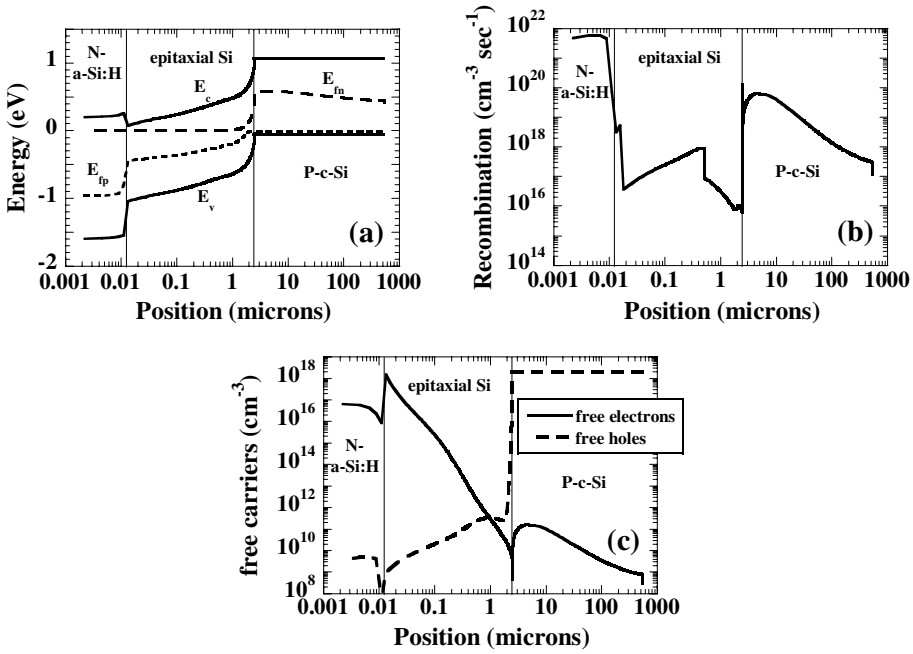

Fig. 5. (a) The energy band diagram, (b) the recombination rate and (c) the free carrier population as a function of position in the device for the solar cell having a 2.4 μm epitaxial silicon intrinsic layer under AM1.5 light and short-circuit conditions.

responsible for the low EQE of the device at long wavelengths. In fact results indicate that electron-hole pairs photo-generated in the front part of the c-Si wafer are collected but not those generated by light deep inside it. To understand this, in Figure 5a we plot the band diagram of the structure, shown schematically in Figure 1. Because of the high electric field at the epi-Si/P-c- Si interface (as evident from Fig. 5a) electrons and holes photo-generated in the front part of the P-c-Si wafer are well-separated. Since the epi-Si layer is of high quality (Tab. 2), the electrons get relatively easy passage through it and are collected at the front contact. The corresponding holes can diffuse through the P-c-Si wafer without recombining, as this wafer is rich in holes. However there is little field in the interior of the c-Si wafer (as maybe inferred from Fig. 5a) to separate the photo-generated carriers, and with the large number of defect states assumed in this heavily P-doped substrate (Tab. 2), considerable recombination occurs (Fig. 5b) resulting in a very low collection from the bulk of the wafer, and consequent low EQE over the longer wavelengths (Figs. 3, 4). It is interesting to note from Figure 5b that the recombination inside the epitaxial silicon layer is lower on either side compared to the centre. This is because of the high field at the interfaces and since there are very few holes available at the front N-a-Si:H/epi-Si interface (because of the strong favourable field here on the holes due to the large valence band discontinuity (ΔE_v) pushing the holes towards the back of the device); and because the free electron population is much lower than that of the free holes at and near the rear epi-Si/P-c-Si interface (Fig. 5c). However, photo-generated hole trapping at the rear interface when the defect density here is high (10^{12} cm^{-2} in this case) produces a large band bending (Fig. 5a) leading to high field very close to the interface and lowering the field over the interior of the epi-Si layer in this 2.4 μm device. Thus the recombination in the interior of the epi-Si layer is high (Fig. 5b). However the strong change in the recombination rate at $\sim$0.5 μm is due to the fact that over a $\sim$0.5 μm region adjacent to the top DL, higher capture cross-sections and defect density than those in the rest of the epi-Si film had to be assumed as already discussed and mentioned in the caption to Table 2.

For comparison we have also shown in red on Figure 4, the calculated values of the light absorbed in the epitaxial Si layer, if it was 5 μm thick (open circles with line) and the corresponding EQE (closed circles with line). We now find that the contribution to the EQE of the device mainly comes from the light absorbed in the thicker epitaxial layer (5 μm), leading to higher currents and efficiency, as will be discussed in Section 5.2.

5.2 What is the optimum thickness of the epi-Si layer for the highest cell efficiency?

The sensitivity of the solar cell output to the thickness of the epi-Si layer is shown in Figure 6, which has been drawn using the parameters of the 2.4 micron cell (Tab. 2), except for the 1.7 μm cell. This is because the thickest (2.4 μm) cell has the best parameters of all the cells so far deposited (Tab. 2 and discussion in Sect. 4). In the case of the 1.7 μm cell, the actual parameters extracted by modeling this case (Sect. 4 and caption of Tab. 2) have been utilised. The abrupt fall in the V_{oc} when the epi-Si layer thickness is 1.7 μm, is due to a higher defect density at the rear epi-Si/P-c-Si interface for this case (Sect. 4). Moreover we have not included the case of 0.9 μm in Figure 6,

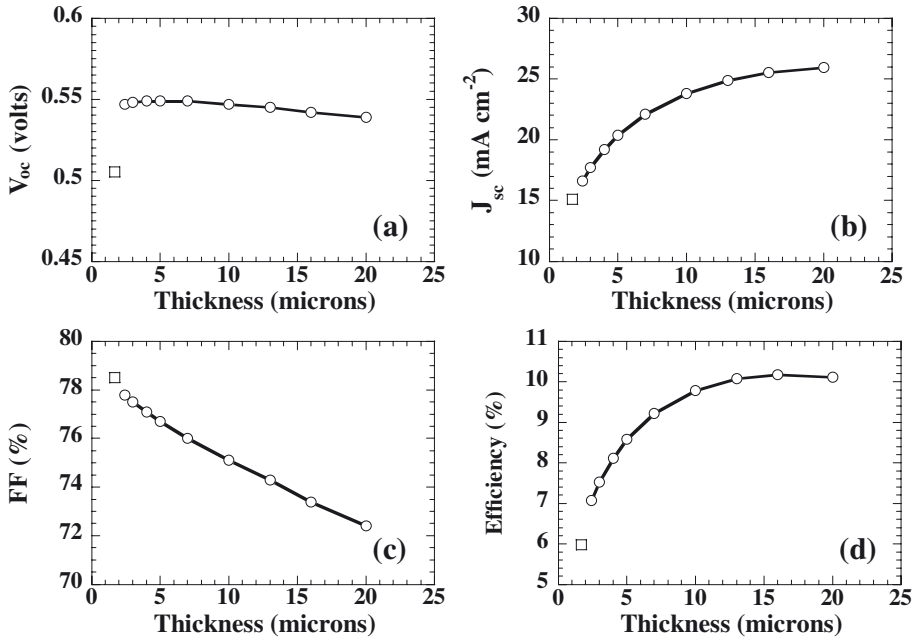

Fig. 6. The solar cell output as a function of the thickness of the epitaxial silicon layer. The sharp fall in V_{oc} of the 1.7 micron cell is due to the fact that modelling of this cell's J-V and EQE characteristics indicate that it has a more disordered interface layer at the epi-Si/P-c-Si interface than is present in the 2.4 micron cell. Therefore a different symbol is used for this case. The thicker cells have been assumed to have the same parameters as the 2.4 micron cell.

as the results of Table 1 indicate an all-round deterioration of cell performance due to a general increase of defect densities for the 0.9 μm cell (Tab. 2 and discussion in Sect. 4). We note from Figure 6d that the efficiency continues to increase up to an epitaxial layer thickness of 17 μm; however, the increase is more prominent for up to 10 microns.

It may be noted that in these results no light-trapping schemes have been considered. The optimum thickness of 17 μm is likely to be radically reduced when one or both surfaces of the epi-Si layer is textured.

5.3 Sensitivity of the solar cell output to the defect states at the rear epi-Si/P-c-Si interface and to those at the front N-a-Si:H/epi-Si interface

In the first part of Table 3 we show the sensitivity of the solar cell output to the defect states at the rear epi-Si/P-c-Si interface and in the second part, the sensitivity to the front N-a-Si:H/epi-Si interface.

5.3.1 Sensitivity of the solar cell output to the defect states at the rear epi-Si/P-c-Si interface

From Table 3 we note that up to $N_{ss,\,back} = 5 \times 10^{11}$ cm^{-2}, the efficiency remains constant, a slight fall in V_{oc} being compensated by a corresponding increase in FF. Even up to $N_{ss,\,back} = 10^{12}$ cm^{-2}, FF continues to increase, although now it is not fully able to annul the fall in V_{oc} and the efficiency begins to decrease. However beyond a defect density of 10^{12} cm^{-2}, V_{oc}, FF and efficiency fall drastically, only the current remaining unchanged. To understand the sharp fall in V_{oc} beyond $N_{ss,\,back} = 5 \times 10^{11}$ cm^{-2} and especially after 10^{12} cm^{-2}, we plot in Figure 7 the electric field at and near the rear DL of the 2.4 μm epi-Si layer cell under AM 1.5 light and open-circuit condition (Fig. 7a) and in Figure 7b the field in an expanded scale inside the epi-Si layer close to this DL. They indicate that for high values of N_{ss} in this DL on the rear surface of epi-Si, the field is localised, resulting in less field penetration into the epi-Si layer and lowering the V_{oc}.

In Figure 8a we trace the band diagram and in Figure 8b the recombination over the 2.4 μm epi-Si layer under AM1.5 light and *short*-circuit conditions. They indicate a sharp increase in band bending at the epi-Si/P-c-Si interface for the highest $N_{ss,\,back}$, resulting in less field penetration into the bulk of the epi-Si layer. However, it is interesting to note the increase in the FF up to $N_{ss,\,back} = 10^{12}$ cm^{-2}, that is particularly sharp at the latter value of $N_{ss,\,back}$. In order to understand we repeat the recombination plot in Figure 8c, this time focusing on the back defective layer on epi-Si and plot the electric field with the same focus in Figure 8d. From this, it appears that the increased FF at $N_{ss,\,back} = 10^{12}$ cm^{-2} is the effect of competition between recombination in the volume of the epi-Si layer (Fig. 8b) and increased field in the front part of the P-type c-Si wafer (Fig. 8d). We have demonstrated in Section 5.1 that carriers from the front part of the c-Si wafer do contribute to the photo- current in the 2.4 μm epi-Si device. This is also the reason for the constancy of the photo-current even for high values of $N_{ss,\,back}$ (e.g. 10^{13} cm^{-2}), the increased recombination

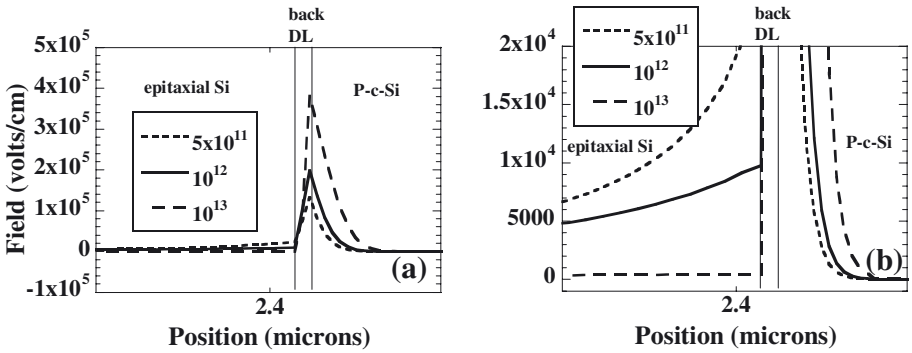

Fig. 7. The electric field (a) inside and near the rear defective layer (DL) on the epi-Si surface and (b) this field shown in an expanded scale inside the epi-Si layer close to this DL, for the 2.4 μm epi-Si layer cell under AM1.5 light and open-circuit conditions with the defect density at the epi-Si/P-c-Si interface as a parameter.

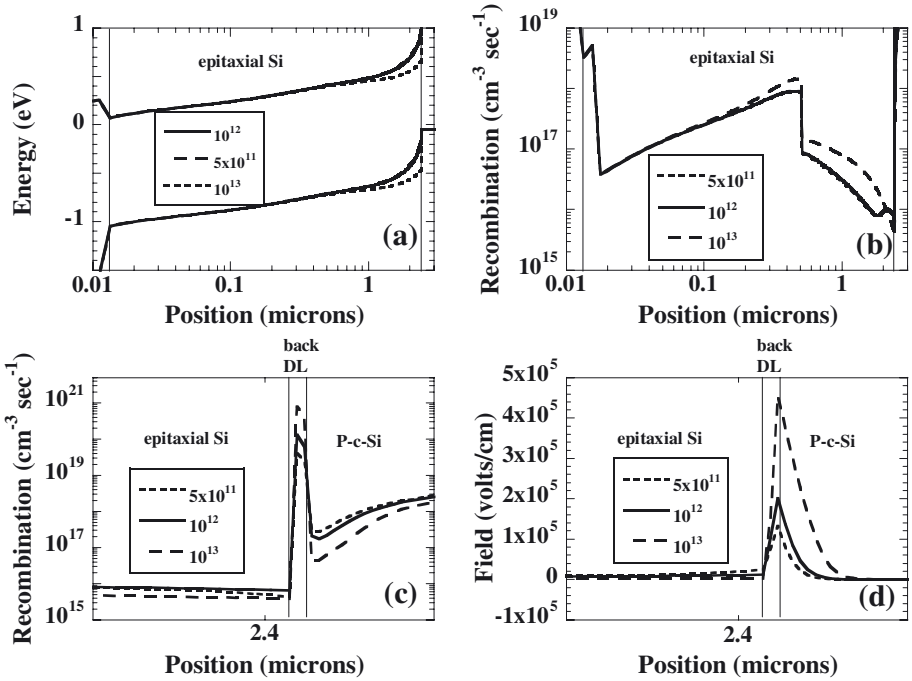

Fig. 8. (a) The energy band diagram, (b) the recombination over the epi-Si layer and (c) around the back interface region; and (d) the electric field over the latter region for the 2.4 μm epi-Si layer cell under AM1.5 light and short-circuit conditions with the defect density at the epi-Si/P-c-Si interface as a parameter.

over the epi-Si layer (Fig. 8b) in this case being compensated for by the higher field (Fig. 8d) and therefore shows decreased recombination (Fig. 8c) over the front part of the c-Si wafer.

To come back to the reasons for the abrupt increase of the FF at $N_{\mathrm{ss,\,back}} = 10^{12}$ cm^{-2}, we note from Figure 8d that with increasing $N_{\mathrm{ss,\,back}}$ the electric field improves appreciably over the front part of the c-Si wafer leading to reduced recombination from this region (Fig. 8c). However for values of $N_{\mathrm{ss,\,back}}$ higher than 10^{12} cm^{-2}, we find from Figure 8b that recombination increases sharply over the volume of the epi-Si layer because of the flattening of the bands (Fig. 8a), so that the extra electrons saved from recombination in the c-Si wafer recombine with back diffusing holes from c-Si inside the epi-Si layer. Thus the collection of carriers and therefore the FF decrease for $N_{\mathrm{ss,\,back}} > 10^{12}$ cm^{-2}. However, up to $N_{\mathrm{ss,\,back}} = 10^{12}$ cm^{-2}, the improved field and hence reduced recombination in the front part of the P-c-Si wafer (Figs. 8d and 8c) is not matched by a corresponding increase of recombination in the epi-Si layer (Fig. 8b), so that the collection of carriers and hence the FF improve.

5.3.2 Sensitivity of the solar cell output to the defect states at the front N-a-Si:H/epi-Si interface

This is shown in the latter part of Table 3. We note that while the solar cell output begins to deteriorate for $N_{\mathrm{ss,\,back}} > 5 \times 10^{11}$ cm^{-2}, in the present case the output is practically unchanged up to $N_{\mathrm{ss,front}} = 10^{12}$ cm^{-2}. The reason for this is as follows: We have already stated

Table 4. Sensitivity to the Gaussian defect density inside the epitaxial silicon layer.

DOS in epi-Si (cm^{-3})	2.4 μm cell			
	J_{sc} (mA cm^{-2})	V_{oc} (V)	FF	Efficiency (%)
10^{13}	16.62	0.558	0.815	7.56
10^{14}	16.62	0.556	0.812	7.51
10^{15}	16.62	0.547	0.778	7.07
5×10^{15}	16.60	0.511	0.721	6.12
10^{16}	16.54	0.484	0.7	5.6
5×10^{16}	15.92	0.410	0.646	4.22
10^{17}	15.19	0.379	0.622	3.58

in Section 4 that the major part of the band discontinuity lies on the valence band side for such PECVD deposited samples. It is this large valence band discontinuity (Fig. 5a) that results in a strong N-a-Si:H/epi-Si beneficial interface field that sweeps the photo-generated holes in the right direction, in other words towards the back P-c-Si/metal contact. Thus there are very few holes near the N-a-Si:H/epi-Si junction (Fig. 5c), resulting in negligible recombination that is responsible for the total lack of sensitivity of J_{sc} to $N_{ss,\,front}$ and of even the V_{oc} and FF up to $N_{ss,\,front} = 10^{12}$ cm^{-2}. It is only when $N_{ss,\,front}$ exceeds 10^{12} cm^{-2} that V_{oc}, FF and hence the efficiency fall sharply.

5.4 Sensitivity to the Gaussian defect density in the epitaxial silicon layer

Since, the macroscopic structural properties of these epi-Si layers are consistent with c-Si [5] we have assumed that as in c-Si, there are no tails in the band gap of this epitaxial silicon layer. The average Gaussian defect density in it as extracted by modelling is 10^{15} cm^{-3} (Tab. 2). We have also shown in Figure 4 that the major contribution to the quantum efficiency even for the 2.4 μm epitaxial silicon cell comes from the epitaxial layer itself. It is therefore only to be expected that there would be a strong sensitivity to this parameter. This is shown in Table 4 and in fact all the solar cell output parameters deteriorate when the defect density inside the epitaxial silicon layer increases. In addition the deposited 2.4 μm cell, whose dangling bond defect density, as extracted by modelling (Tab. 2) is 10^{15} cm^{-3} may in fact attain a FF of 0.812, equal to c-Si or "Heterojunction with Intrinsic Thin layer (HIT)" solar cells, if its dangling bond defect density can be reduced to 10^{14} cm^{-3}.

5.5 Cumulative improvement of the epitaxial silicon solar cell output as predicted by modelling

In this sub-section we begin with the solar cell output parameters already attained in the deposited solar cells and point out the improvements suggested by modelling. In the process we also briefly describe the effect of randomly texturing one or both faces of the epitaxial silicon layer on device performance, using the optical model integrated into ASDMP [8]. In the model a ray impinging on a rough interface is divided into 4 components – specular reflection and transmission obeying the Fresnel's law and diffused reflection and transmission that in general have both angular and wavelength dependence. For the diffused components, coherence is assumed to be lost, so that the point where the light impinges is like a new source emitting in all directions. However no wavelength dependence is assumed for the rear textured interface (epi-Si/P-c-Si) at present in this model. Cumulative improvement of the cell output is given in Table 5.

We find that increasing the epi-Si layer thickness to 5 μm increases the current output of the device, and although the FF falls slightly, there is a net gain in efficiency of 1.5%. Our experimental group has recently been successful in depositing epi-Si layers 5 μm thick (not yet reported). Therefore we hold this thickness constant for the subsequent improvement steps. Diminution of the epi-Si/P-c- Si interface defect density ($N_{ss,\,back}$) from 10^{12} cm^{-2} to a moderate 5×10^{11} cm^{-2} mainly brings up the V_{oc}. Thereafter we initially consider the effect of randomly texturing only the top N-a-Si:H/epi-Si interface and finally both the top and bottom interfaces of the epi-Si layer. The resultant increase in the short-circuit current density leads to a final J_{sc} of 29.21 mA cm^{-2} and an efficiency of 13.02% for a 5 μm thick epi-Si layer solar cell. In fact the final current level achievable compares favourably with that of mono-c-Si solar cells.

Table 5 indicates that with light trapping effects in place, we can now achieve satisfactory values of both J_{sc} and FF. Only the V_{oc} is still far inferior to HIT solar cells. In fact the structure studied is a NIP solar cell, the emitter being N-a-Si:H. It is known that due to a more favourable band diagram, the reverse structure PIN (emitter P-a-Si:H), that is, when the epi-Si layer is deposited on a highly N-doped c-Si substrate, should have a higher V_{oc} (higher built-in potential) although at the cost of a lower FF, because in this case the valence band discontinuity would act to hamper hole extraction from the device. It may however be pointed out that the final aim of depositing such epi-Si solar cells is to lift the epi-Si film off the c-Si wafer, thus leading to cost saving from wafer reuse. When this is done both the epi-Si film deposited on the P-type wafer and that deposited on the N-type wafer would have valence band discontinuities from amorphous contacts deposited at both ends. In fact the resultant epi-Si cells would have double hetero-junctions, one at either end of the epi-Si layer. In such cases, the valence band discontinuity hampers hole collection either at the emitter or the BSF ends. Thus the FF advantage of the NIP structure would be lost. However the superior V_{oc} potential of the PIN structure would remain, so that a PIN structure epi-Si solar cell is expected to also show an improved V_{oc}.

6 Conclusions

We have simulated a thickness series of epitaxial silicon solar cells grown on a highly doped P-type c-Si substrate,

Table 5. Cumulative improvement of the solar cell output parameters by improving various device and material parameters. The parameter that is improved at each stage leading to a higher efficiency, is given in bold italics.

Different solar cell input parameters	J_{sc} (mA cm^{-2})	V_{oc} (V)	FF	Efficiency (%)
Cell deposited experimentally (2.4 μm epi-Si layer) – all flat interfaces	16.60	0.546	0.77	7.00
Model results for the above cell	16.63	0.547	0.778	7.07
Epitaxial layer thickness = 5 μm	***20.35***	0.549	0.767	8.57
$N_{ss,\,back}$ reduced to 5×10^{11} cm^{-2}	20.36	***0.580***	0.747	8.83
N-a-Si:H/epi-Si interface textured	***25.53***	0.589	0.750	11.27
Both top & bottom of epi-Si textured	***29.21***	0.594	0.750	13.02

with a flat ITO/N-a-Si:H window design. We have assumed that the macroscopic structural properties of the epi-Si film, such as the band gap, no band tails and the complex refractive indices are the same as that of c-Si, based on experimental findings on the epi-Si films [5]. Modelling indicates that optimised parameters are not attained in this type of solar cells for thickness $\leqslant$1.7 μm of the epi-Si film, while the 2.4 μm deposited cell has low interface and bulk defect densities. However for the current in this N-a-Si:H/I-epi-Si/P$^+$-c-Si structure to come almost entirely from the epi-Si film, we need to increase the epitaxial silicon layer thickness further, to at least 5 μm. Simulations also reveal that solar cell output is more sensitive to the defect states at the rear epi-Si/P-c-Si interface than to those at the top N-a-Si:H/epi-Si junction, mainly because the valence band discontinuity at the latter interface yields a strong favourable field that aids hole collection. Using model ASDMP to calculate the sensitivity of the solar cell output to various device parameters, we show that an efficiency of 8.83% is practically attainable with a 5 μm epi-Si layer, which maybe increased further to 13.02% by introducing suitable light-trapping effects, thus increasing J_{sc} to 29.21 mA cm^{-2}. Final optimisation results presented in Table 5 indicate that V_{oc} still remains inferior to HIT solar cells. The inverse structure, with the epi-Si layer grown on a heavily doped N-type c-Si wafer needs to be studied experimentally and by modelling and may hold out promise of improved V_{oc} and a further gain in conversion efficiency.

This study was funded by the Ministry of New and Renewable Energy, Government of India, and by the *Centre National de la Recherche Scientifique* (CNRS), France. The computer modelling program was initially developed (electrical part) by P. Chatterjee during the course of a project funded by MNRE and DST, Government of India, and the optical part was added during her tenure as Marie Curie fellow *École Polytechnique*, Palaiseau, France. It was extended to model also HIT cells under a CSIR project.

References

1. R.B. Bergmann, C. Berge, T.J. Rinke, J. Schmidt, J.H. Werner, Sol. Energy Mater. Sol. Cells **74**, 213 (2002)
2. I. Kuzma-Filipek, K.V. Nieuwenhuysen, J.V. Hoeymissen, M.R. Payo, E.V. Kerschaver, J. Poortmans, R. Mertens, G. Beaucarne, E. Schmich, S. Lindekugel, S. Reber, Prog. Photovolt.: Res. Appl. **18**, 137 (2010)
3. K. Alberi, I.T. Martin, M. Shub, C.W. Teplin, M.J. Robero, R.C. Reedy, E. Iwaniczko, A. Duda, P. Stradins, H.M. Branz, D.L. Young, Appl. Phys. Lett. **96**, 073502 (2010)
4. H. Petermann et al., Prog. Photovolt.: Res. Appl. **20**, 1 (2012)
5. R. Cariou, M. Labrune, P. Roca i Cabarrocas, Sol. Energy Mater. Sol. Cells **95**, 2260 (2011)
6. M. Moreno, D. Daineka, P. Roca i Cabarrocas, Phys. Stat. Sol. C **7**, 1112 (2010)
7. M. Moreno, P. Roca i Cabarrocas, EPJ Photovoltaics **1**, 10301 (2010)
8. P. Chatterjee, M. Favre, F. Leblanc, J. Perrin, Mat. Res. Soc. Symp. Proc. **426**, 593 (1996)
9. M. Nath, P. Chatterjee, J. Damon-Lacoste, P. Roca i Cabarrocas, J. Appl. Phys. **103**, 034506 (2008)
10. P. Roca i Cabarrocas, J.B. Chevrier, J. Huc, A. Lloret, J.Y. Parey, J.P.M. Schmitt, J. Vac. Sci. Technol. A **9**, 2331 (1991)
11. P. Chatterjee, J. Appl. Phys. **76**, 1301 (1994)
12. P. Chatterjee, J. Appl. Phys. **79**, 7339 (1996)
13. P.J. McElheny, J.K. Arch, H.-S. Lin, S.J. Fonash, J. Appl. Phys. **64**, 1254 (1988)
14. J.P. Kleider, A.S. Gudovskikh, P. Roca i Cabarrocas, Appl. Phys. Lett. **92**, 162101 (2008)
15. F. Leblanc, J. Perrin, J. Schmitt, J. Appl. Phys. **75**, 1074 (1994)
16. J.M. Essick, J. David Cohen, Appl. Phys. Lett. **55**, 1232 (1989)
17. H. Matsuura, T. Okuno, H. Okushi, K. Tanaka, J. Appl. Phys. **55**, 1012 (1984)
18. H. Mimura, Y. Hatanaka, Appl. Phys. Lett. **50**, 326 (1987)

Cite this article as: S. Chakraborty, R. Cariou, M. Labrune, P. Roca i Cabarrocas, P. Chatterjee, Feasibility of using thin crystalline silicon films epitaxially grown at 165 °C in solar cells: A computer simulation study, EPJ Photovoltaics **4**, 45103 (2013).